INSTITUTE OF PHYSICS PUBLISHING JOURNAL OF PHYSICS: CONDENSED MATTER

J. Phys.: Condens. Matter **14** (2002) 447–459 PII: S0953-8984(02)28185-0

Optical spectroscopy of Al_2O_3:Ti^{3+} single crystal under hydrostatic pressure. The influence on the Jahn–Teller coupling

S García-Revilla[1], F Rodríguez[1,3], R Valiente[1] and M Pollnau[2]

[1] DCITIMAC, Facultad de Ciencias, Universidad de Cantabria, 39005 Santander, Spain
[2] Institute of Applied Optics, Department of Microtechnique, Swiss Federal Institute of Technology, CH-1015 Lausanne, Switzerland

E-mail: rodriguf@unican.es

Received 22 August 2001, in final form 13 November 2001
Published 21 December 2001
Online at stacks.iop.org/JPhysCM/14/447

Abstract

This work investigates the effect of hydrostatic pressure on the excitation and emission spectra, as well as on the lifetime, of Al_2O_3:Ti^{3+} at room temperature. The aim is to establish correlations between the pressure-induced band shifts and the corresponding local structural changes undergone by the TiO_6 complex. A blue-shift of 8.52 and 6.86 cm^{-1} $kbar^{-1}$ was found for the lower (E_1) and upper (E_2) energy components of the excitation band at 17 760 and 20 500 cm^{-1}, respectively, and blue-shifts of 5.93 and 5.40 cm^{-1} $kbar^{-1}$ for the two overlapping bands of the emission spectrum located at 12 680 and 14 210 cm^{-1}. We explain these results on the basis of a reduction of the TiO_6 Jahn–Teller distortion upon increasing the pressure. In contrast, the increase of the overall Stokes shift, which is mainly associated with electron–vibration coupling to the totally symmetric a_{1g} vibration, is explained by the increase of the excited-state stabilization energy, $S_{a_{1g}}\hbar\omega_{a_{1g}}$, with increasing pressure.

The luminescence lifetime is also found to be pressure dependent, varying from 2.6 μs at ambient conditions to 3.2 μs at 80 kbar. This increase is caused by a diminution of the transition oscillator strength that is related to the odd-vibration assistance mechanism. The softening of the transition mechanism is interpreted in terms of the blue-shift experienced by the $O^{2-} \rightarrow Ti^{3+}$ charge-transfer transition energy upon increasing the pressure.

1. Introduction

Tunable near-infrared (NIR) solid-state laser materials are essential for technological applications in telecommunications, femtosecond spectroscopy, sensors, and medicine. The

[3] Author to whom any correspondence should be addressed.

success of titanium-doped sapphire (Al_2O_3:Ti^{3+}) as a tunable solid-state laser in the red–NIR range was first demonstrated in 1982 [1]. The need for wide-range tunable lasers has motivated the search for new host lattices for Ti^{3+} [2,3] as well as for new ions capable of showing broad-band NIR laser action. In fact, transition metal ions such as Ni^{2+}, Cr^{2+}, Cr^{4+}, and Mn^{5+} have been intensively investigated for such purposes [4–7]. However, a proper understanding of the laser capability of these materials still requires an adequate microscopic characterization of the different spectroscopic contributions. In particular, the contributions to the emission and excitation Stokes shift are related to the electron–vibration couplings between the ground and excited states involved in the electronic transition, and the associated equilibrium geometries. The present paper deals with the investigation of these processes in Al_2O_3:Ti^{3+}. Actually, Ti^{3+} has the simplest electronic configuration ($3d^1$), outside the closed-shell ions, among transition metal (TM) ions. A first-order approximation of the electronic structure of Ti^{3+}-doped sapphire can be made on the basis of the trigonal symmetry (nearly octahedral) of the substituting Al^{3+} site [8, 9]. The ^2D electronic free-ion ground state splits into a doublet ^2E_g excited state and a triplet $^2T_{2g}$ ground-state level in an octahedral crystal field. The only d–d $^2T_{2g} \rightarrow {}^2E_g$ electronic transition is very sensitive to the crystal-field strength, $10Dq$, yielding a broad band associated with the different equilibrium geometries of the electronic ground state and excited state, as a consequence of the linear electron–vibration coupling with the totally symmetric a_{1g} mode. In the configurational-coordinate model, the minimum of the ^2E_g excited-state potential energy is shifted with respect to the potential energy of the $^2T_{2g}$ ground state towards larger Ti–O distances due to the strong electron–vibration coupling, resulting in a large Stokes shift. Nevertheless, the success of Ti^{3+} for laser action is enhanced by the Jahn–Teller (JT) effect. The ^2E_g and $^2T_{2g}$ electronic states are both orbitally degenerate. Thus there must be low-symmetry structural distortions of the TiO_6 complex, leading to lower-energy configurations (JT theorem [10, 11]). This effect, which is clearly evidenced by the double-humped structure exhibited by the absorption and luminescence bands, provides an additional contribution to the Stokes shift, thereby improving the four-level laser action of this material. This characteristic, shown as a broad absorption band, favours efficient pump excitation into the ^2E_g excited state, as well as a broad emission band yielding a very broad laser tuning range (670–1100 nm). The small trigonal components of the crystal field in Al_2O_3:Ti^{3+} partially lift the degeneracy of the $^2T_{2g}$ state (not that of the ^2E_g state) [8,9], but do not play a significant role in the spectroscopic properties associated with the broad-band structure of this material. Interestingly, the total splitting of the ground state induced by the trigonal field and (mainly) the JT distortion is only a few hundreds of wavenumbers, whereas the splitting for the ^2E excited state into $^2A_{1g}$ and $^2B_{1g}$ (D_{4h} notation), which is mostly due to the strong $E \otimes e$ JT effect, amounts to 2740 cm^{-1}.

The luminescence lifetime of Ti^{3+}-doped oxide crystals is only a few microseconds [12]. As for most transition metal complexes, these lifetime values are characteristic of d–d crystal-field transitions involving electronic states of the same spin [13]. Although the basic properties of Ti^{3+}-doped sapphire have been known for many years [8, 9, 14], recent studies devoted to obtaining an understanding of both the pure radiative mechanisms and multiphonon relaxation phenomena, as well as the influence of the strong $E \otimes e$ JT effect on these processes [15, 16], illustrate the relevance of this fundamental as well as applied material.

The aim of this work is to investigate the optical properties of Al_2O_3:Ti^{3+} under pressure. In particular, attention is paid to the variation of the electron–vibration couplings related to the totally symmetric, a_{1g}, and the JT-active, e_g, vibrational modes as a function of volume, i.e. Ti–O distance, R.

We have carried out excitation and luminescence measurements under hydrostatic pressure in the 0–110 kbar range. This aspect is crucial to elucidating the contribution of these two electron–vibration couplings as a function of the crystal volume. Previous spectroscopic

works under pressure on Al_2O_3:Ti^{3+}, which used optical absorption spectroscopy [17] and luminescence spectroscopy at low temperatures [18], did not deal with these phenomena in conveniently hydrostatic conditions. In the latter case, the luminescence spectra were taken under non-hydrostatic conditions with significant axial stress. This aspect is important, since axial components can additionally enhance the low-symmetry distortion of the TiO_6 complex beyond the JT effect. In this work we present a complete study of the excitation and luminescence spectra of Al_2O_3:Ti^{3+} under pressure. The results are interpreted in terms of a simple model based on the linear electron–vibration coupling by the a_{1g} vibrations as well as by the $E \otimes e$ JT effect. In this study we show that the application of hydrostatic pressure can improve the laser performance, as is reflected by the increase of the luminescence lifetime with pressure. In addition, it provides a continuous luminescence shift to higher energies, extending the potential tuning range to shorter wavelengths (about 30 nm in 100 kbar).

2. Experimental procedure

Microsamples of Al_2O_3 doped with 0.35 mol% Ti^{3+} were grown by the Kyropoulos technique. The actual Ti^{3+} concentration was obtained from the absorption coefficient of the single crystal investigated (size $10 \times 3 \times 7$ mm^3). Hydrostatic pressure experiments were carried out in a diamond-anvil cell (High Pressure Diamond Optics, Incorporated), using a 16:3:1 methanol–ethanol–H_2O mixture as the pressure-transmitting medium. We used preindented Inconel gaskets machined with a Natjet model microdrill (hole diameter $= 250\ \mu$m). The crystal sizes were about $50 \times 120 \times 70\ \mu$m^3. The 530.9 nm line of a Kr^+-ion laser (Coherent CR-500 K) was used to pump the Ti^{3+} ions into the ^2E_g excited state (O_h notation). We employed a Jobin–Yvon U1000 double monochromator for dispersing the luminescence spectra at an excitation power of 30 mW. The excitation spectra were obtained by means of a photoluminescence set-up that was especially designed for detecting very weak luminescence signals. We used a tungsten lamp and an Acton Research Corporation SpectraPro–300i monochromator as excitation sources. The excitation light was focused onto the hydrostatic cavity through an Ealing 30× reflective objective. In order to improve the detection sensitivity (signal-to-noise ratio), the luminescence was passed through an Oriel interferential filter centred at 741 nm with a full width of 81 nm, using a Hamamatsu R4457P low-noise phototube and a Stanford Research SR400 photon counting system. This procedure provided suitable excitation spectra in the 400–700 nm range. The operation at long wavelengths was limited by the detection system. The luminescence from the Al_2O_3:Ti^{3+} microcrystal investigated was 1000 photons s^{-1} at the band maximum. The luminescence and excitation spectra have been corrected for instrumental response. Pressure for the excitation and luminescence spectra was measured through the first-order Raman shift of silicon chips, peaked at 520 cm^{-1} at ambient pressure. This sensor avoids unwanted luminescence signals emerging from ruby chips, that can completely mask the broad-band excitation spectra of Al_2O_3:Ti^{3+}. Initial calibration was accomplished on the single Si microcrystals employed in these experiments by use of the pressure scale of ruby (figure 1). We obtain a relation between the Raman shift (S_R, cm^{-1}) and pressure (P, kbar) of $S_R = 519.3 + 0.56P - 1.3 \times 10^{-3}P^2$. By fitting the pressure as a function of the Raman shift, we obtain an analogous equation: $P = 1.51 + 1.70(S_R - 520) + 0.014(S_R - 520)^2$, which has been employed for pressure calibration. This provides a pressure sensitivity at $P = 0$ of 0.56 cm^{-1} kbar^{-1} which is slightly higher than the value of 0.54 cm^{-1} kbar^{-1} given in [19]. Nevertheless, a similar value is also obtained from the data of figure 1 if a linear fit is considered.

Rectangular excitation pulses for the lifetime experiments were generated by passing the laser beam through an acousto-optic modulator (Newport EOS-AOM) connected to a function

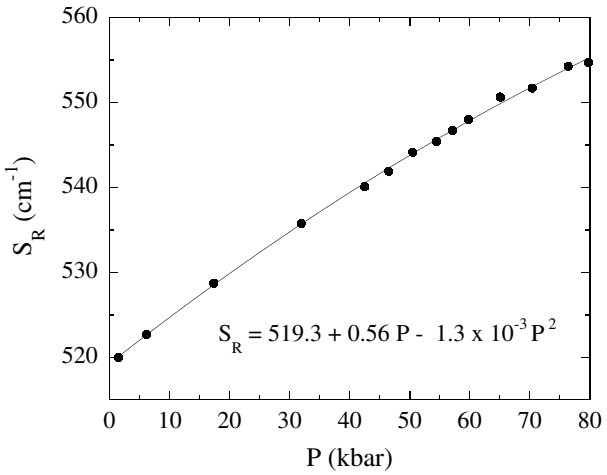

Figure 1. The dependence of the first-order silicon Raman shift, S_R, on pressure at 293 K. Pressure values were obtained from the shift of the ruby R lines. The full curve represents a least-squares fit to a quadratic function.

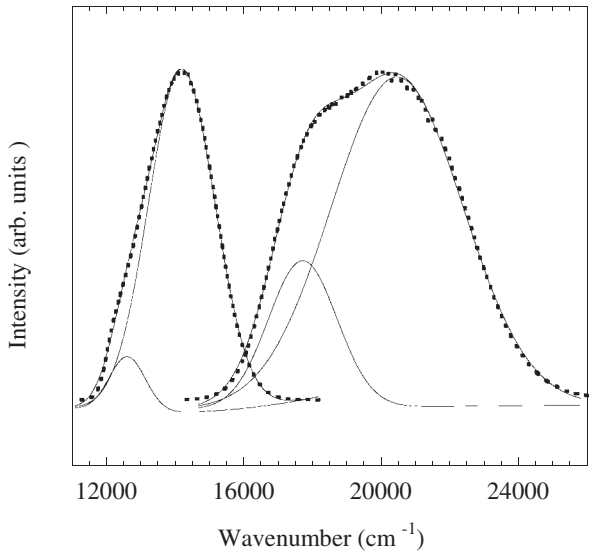

Figure 2. Excitation (right) and luminescence (left) spectra (dots) of Al_2O_3:Ti^{3+} obtained for a macroscopic sample of $10 \times 3 \times 7$ mm^3 at ambient conditions (293 K and 1 bar). Solid curves are fits of the experimental data to the sums of two Gaussians.

generator (HP 3325 A Synthesizer). The luminescence signal was analysed with a digital scope (Tektronix 2430A).

3. Results and analysis

Figure 2 shows the luminescence and corresponding excitation spectra of 0.35 mol% Ti^{3+}-doped Al_2O_3 under ambient conditions. Each spectrum consists of a broad band exhibiting a

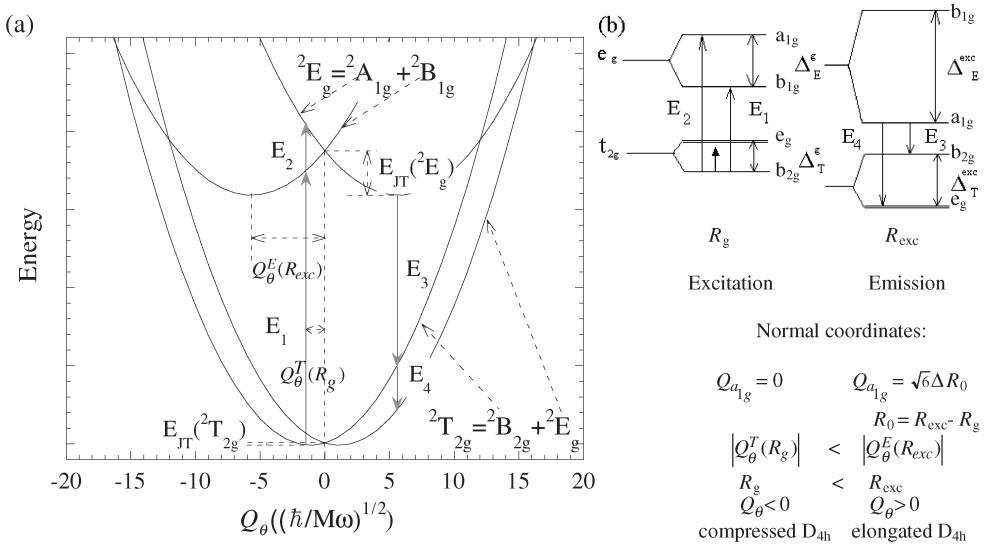

Figure 3. (a) A configurational-coordinate diagram for the TiO_6 complex. E_1 and E_2 (E_3 and E_4) indicate the electronic transition energies for the transitions between the ground- (excited-) state minimum and the excited (ground) state. The displacement of the minimum as a function of the linear electron–vibration coupling constant and the vibrational frequency is given in the text. Note that the ground-state JT minimum ($T_2 \otimes e$) corresponds to a compressed octahedron geometry ($Q_\theta^T < 0$) while for the excited state ($E \otimes e$) it corresponds to an elongated D_{4h} geometry ($Q_\theta^E < 0$) with $|Q_\theta^T| < |Q_\theta^E|$ (in this diagram the vibronic Q_ε-coordinate is taken as $Q_\varepsilon^T = Q_\varepsilon^E = 0$). (b) One-electron energy-level diagrams of the d levels in a tetragonal symmetry produced by the octahedral crystal field and the JT effect. The excitation and emission transitions are indicated by arrows. The splitting corresponds to the $T_2 \otimes e$ JT effect with an associated compressed geometry ($Q_\theta^T < 0$, left), while it corresponds to the $E \otimes e$ JT effect in the ^2E_g excited state with ($Q_\theta^E < 0$, right). The greater splitting on the right is due to the greater coupling associated with ^2E_g with respect to $^2T_{2g}$.

double-humped structure. The band shape can be well described with two Gaussians peaked at 12 680 (E_3) and 14 210 cm^{-1} (E_4) for luminescence, and at 17 760 (E_1) and 20 500 cm^{-1} (E_2) for excitation (figure 2). The configurational-coordinate potential-energy diagrams for the octahedral ^2E_g electronic ground state and the $^2T_{2g}$ electronic excited state coupled with the JT e_g (Q_θ, Q_ε) vibration is given in figure 3(a). Similar diagrams were used in [15] for describing band shapes. The electronic transitions between the ^2E_g and $^2T_{2g}$ parent octahedral states that are split by the JT distortion are indicated for excitation and luminescence in figure 3(b). Note that the transition energy roughly represents the crystal-field splitting $10Dq$, $^2T_{2g} \rightarrow {}^2E_g$, of the nearly octahedral TiO_6 complex formed. The double-humped structure observed in figure 2 is associated with axial distortions related to the JT effect of the $3d^1$ configuration according to the energy-level diagram of figure 3(b). Values of the crystal-field splitting $10Dq$ and the JT splitting for the ^2E_g excited state in the equilibrium geometry of the $^2T_{2g}$ electronic ground state (distance R_g): $\Delta_E^g(R_g)$ and for the $^2T_{2g}$ ground state in the equilibrium geometry of the ^2E_g excited state (distance R_{exc}): $\Delta_T^{exc}(R_{exc})$, deduced from the spectra of figure 2, are

$$10Dq = 19\,130\ cm^{-1}$$
$$\Delta_E^g(R_g) = 2740\ cm^{-1}$$
$$\Delta_T^{exc}(R_{exc}) = 1530\ cm^{-1}.$$

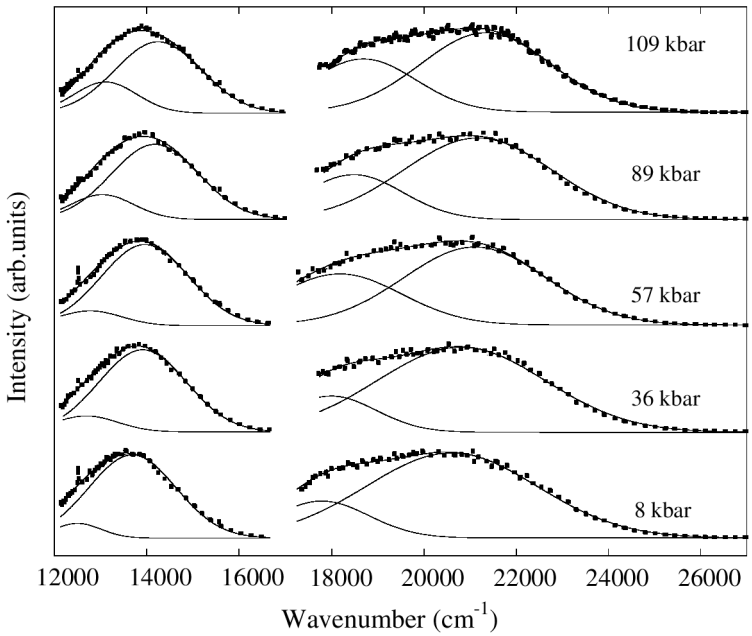

Figure 4. Variation of the emission and excitation spectra of Al_2O_3:Ti^{3+} with hydrostatic pressure at 293 K. Single-crystal dimensions: $50 \times 120 \times 70$ μm^3. The spectra have been fitted to the sums of two Gaussians in the same way as those of figure 3. Solid curves correspond to the least-squares fits; dots show the experimental data.

R_g and R_{exc} correspond to the *average* Ti^{3+}–O^{2-} distances of the TiO_6 octahedron in the $^2T_{2g}$ ground state and the ^2E_g excited state, respectively. Strictly, we should reduce the given $10Dq$ value by $2E_{JT} = (2/3)\Delta_T^g(R_g)$ corresponding to the $^2T_{2g}$ ground state, which is estimated to be 400 cm^{-1} [18].

The variation of the excitation and luminescence bands with hydrostatic pressure in the 0–110 kbar range is shown in figure 4. The pressure range is limited by the hydrostaticity of the pressure-transmitting medium. Note that the low-energy limit of the excitation spectra (17 240 cm^{-1}) is imposed by the detection system employed in the experiments (see the experimental section).

The variation of the corresponding transition energies with pressure is plotted in figure 5. The four components depend linearly on pressure and exhibit pressure blue-shifts of: $E_1(P) = 17\,690 + 8.52P$; $E_2(P) = 20\,590 + 6.86P$; $E_3(P) = 12\,450 + 5.93P$; and $E_4(P) = 13\,670 + 5.40P$, where P and E are expressed in kbar and cm^{-1}, respectively. The splittings for excitation and emission, respectively, that are associated with the JT effect and the trigonal crystal-field components are given by

$$\Delta_E^g(R_g) = E_2 - E_1 = 2900 - 1.66P$$
$$\Delta_T^{exc}(R_{exc}) = E_4 - E_3 = 1220 - 0.53P.$$

Both splittings decrease upon increasing the pressure. This result is noteworthy since recent pressure investigations carried out on $Cs_2NaSrCl_6$:Cr^{3+} [20,21] showed that the JT energy for the $^4T_{2g}$ excited state decreases with increasing pressure, in agreement with our findings, where a clear decrease of the JT splitting is observed for both the excited and ground electronic states upon increasing pressure. On the other hand, the variation of the centroid of the bands, which provides the value of $10Dq$ directly, indicates that this parameter increases with increasing

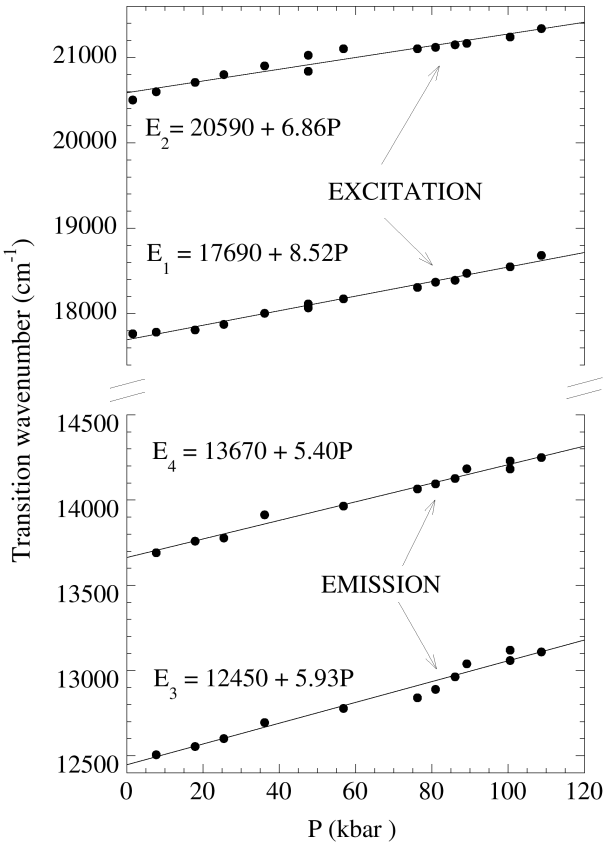

Figure 5. Variation of the peak energies corresponding to the emission and excitation band components of Al_2O_3:Ti^{3+} with pressure. The solid lines represent linear fits to the experimental data.

pressure at a rate of 7.7 cm^{-1} $kbar^{-1}$ as expected for a reduction of the Ti^{3+}–O^{2-} distance with pressure. However, this pressure dependence of $10Dq$ is smaller than the variation estimated on the basis of $10Dq \propto R_g^{-5}$ [22]. Taking into account that the sapphire bulk modulus is $B_0 = 2510$ kbar [23], $R_g \approx 1.9$ Å, and $10Dq = 19\,130$ cm^{-1}, we obtain

$$\left(\frac{\partial 10Dq}{\partial P}\right)_{T,P=0} = \left(\frac{\partial 10Dq}{\partial R}\right)_T \left(\frac{\partial R}{\partial P}\right)$$
$$= -5\frac{10Dq}{R_g}\left[-\frac{R_g}{3B_0}\right] = \frac{5}{3} \times \frac{19\,130}{2510} = 12.7 \text{ cm}^{-1} \text{ kbar}^{-1}. \quad (1)$$

This value is somewhat higher than the experimental value, reflecting a smaller compressibility for the TiO_6 complex than for the AlO_6 octahedron host. The reason is that the size of the Ti^{3+} ion is larger than that of the Al^{3+} ion. This implies an already partly compressed octahedron in the locality of a Ti^{3+} impurity within the Al_2O_3 host and, hence, a smaller residual compressibility. The value obtained experimentally can be conciliated with an R-dependence of $10Dq \propto R^{-5}$ if we assume that $B_{\text{local}} \approx 4100$ kbar. This result is similar to findings on Al_2O_3, MgO:Cr^{3+}, and other related oxides, where the local bulk modulus of CrO_6 is estimated to be 26% higher than that of the host crystal [24]. Higher values were obtained by Zheng for Cr^{3+}-doped $Y_3Al_5O_{12}$, $Gd_3Ga_5O_{12}$, and $Gd_3Sc_2Ga_3O_{12}$ [25, 26].

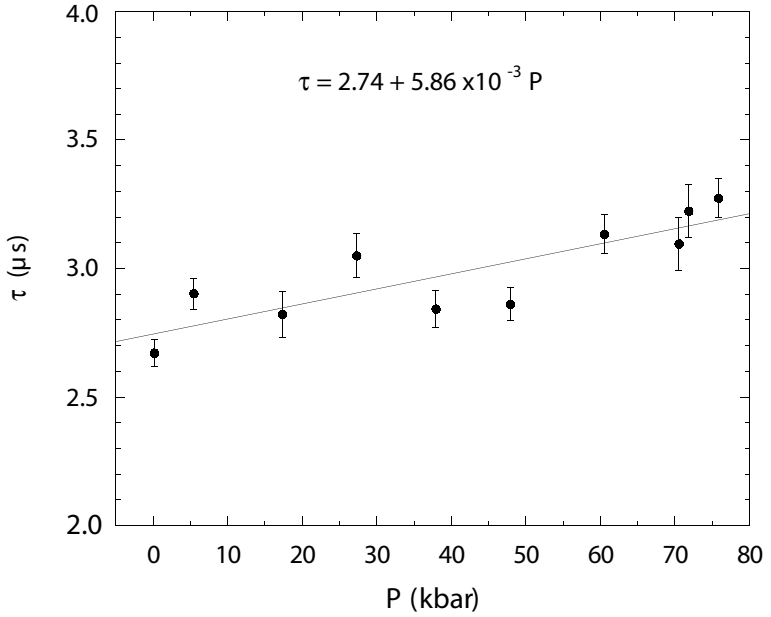

Figure 6. Pressure dependence of the $^2E_g \rightarrow {}^2T_{2g}$ luminescence lifetime, $\tau(P)$, of Al_2O_3:Ti^{3+} at room temperature. The solid line is the least-squares linear fit to the experimental data.

Figure 6 shows the variation of the luminescence lifetime with pressure. An increase of lifetime of 0.6 μs is observed when increasing the pressure from ambient pressure to 80 kbar. The dependence of τ on P is found to be linear with a rate of 5.86×10^{-3} μs kbar^{-1}. This pressure enhancement of the lifetime potentially improves the laser capability of this material.

4. Discussion

As mentioned above, the emission and excitation spectra at ambient pressure and temperature of doped Al_2O_3:Ti^{3+} can be explained on the basis of a simple octahedral TiO_6 complex, through linear electron–vibration couplings to the totally symmetric a_{1g} vibration and the JT e_g (Q_θ, Q_ε) vibrational mode. Although the vibration of the t_{2g} symmetry can also be coupled to the $^2T_{2g}$ electronic state, the influence of this coupling is expected to be much smaller than that of the coupling provided by e_g vibrations [10]. The JT interaction in octahedral coordination for the $^2T_{2g}$ ground state is only a π-effect and hence rather weak, while it is much stronger for the ^2E_g excited state, in view of the σ-character of that bonding.

Figure 3(a) depicts the potential energy for the $^2T_{2g}$ and ^2E_g states as a function of the configuration coordinate Q_θ (e_g vibration). Within this diagram, two transitions are possible for excitation (E_1 and E_2) and for emission (E_3 and E_4). As already pointed out, this is clearly reflected in the optical spectra through the two-component band structure. It must be noted that this pattern applies for the so-called intermediate and strong JT coupling ($S \geqslant 1$) independently of whether the JT regime is static or dynamic. The splitting between these

two components provides direct access to the JT distortion of the complex in their respective electronic ^2E_g (excitation) and $^2T_{2g}$ (emission) states. It is noteworthy that the JT splittings of the two bands are of the same order:

$$\Delta_E^g(R_g) = 2740\ \text{cm}^{-1} \qquad \text{for excitation}$$

and

$$\Delta_T^{exc}(R_{exc}) = 1530\ \text{cm}^{-1} \qquad \text{for emission.}$$

This is an apparently puzzling feature, given that the linear electron–vibration coupling of ^2E_g is stronger than that of $^2T_{2g}$ due to the σ-bonding character of the e_g orbitals as compared to the π-bonding t_{2g} orbitals. The corresponding JT splittings, which are denoted by Δ_E and Δ_T in figure 3, respectively, have been measured for the same coordination geometry as a function of Q_θ for MnF_6^{3-} complexes through the A_nMnF_{n+3} (with $n = 1, 2, 3$) crystal series of compounds with different dimensionality [27]. Values of $\Delta_T = 10\,200\,Q_\theta$ and $\Delta_E = 41\,000\,Q_\theta$ (cm^{-1} Å^{-1}) were obtained for the $^5B_{1g}$ ground-state equilibrium geometry through the Mn^{3+} series, leading to a ratio $\Delta_E/\Delta_T \approx 4$ [27]. The variation of the Δ_E splitting for Cu^{2+} in $CuCl_6^{4-}$, as obtained from a series of Cu chlorides, is $\Delta_E = 18\,200\,Q_\theta$ [28]. This value is approximately two times smaller than that for MnF_6^{3-}. Apart from the different natures of the metal and ligand-forming complexes, this probably reflects the increase of the respective coupling constants with decreasing metal–ligand distances (complex volume) [27, 28]. For Ti^{3+}, a band-shape analysis carried out by Jia *et al* [18] gives $\Delta_E^g(R_g) = 2490\ \text{cm}^{-1}$ and $\Delta_T^g(R_g) = 670\ \text{cm}^{-1}$. These values provide a ratio of $\Delta_E^g(R_g)$ to $\Delta_T^g(R_g)$ that is close to 4, in good agreement with the experimental ratio measured for the Mn^{3+} fluoride series [27].

The band splitting observed in the excitation and luminescence spectra at ambient pressure can be interpreted on the assumption that $\Delta_E^g \approx 4\Delta_T^g$, taken together with the fact that the vibrational frequencies for excited and ground states depend on the complex volume as $\partial \ln(\omega)/\partial \ln(V) = -\gamma$. Here, γ is the Grüneisen parameter, whose mean value is $\gamma = 1.31$ for Al_2O_3 [23].

Within a model of linear electron–vibration coupling between the $^2T_{2g}$ and ^2E_g electronic states with vibrations of a_{1g} and e_g symmetry (O_h scheme), the four components of the emission and excitation transitions, shown in figure 3, can be written as

$$\begin{aligned}
E_1 &= 10Dq^g - \tfrac{1}{2}\Delta_E^g + \tfrac{2}{3}\Delta_T^g = 10Dq^g - \tfrac{1}{2}|A_1^E Q_\theta^T| + \tfrac{2}{3}|A_1^T Q_\theta^T| \\
E_2 &= 10Dq^g + \tfrac{1}{2}\Delta_E^g + \tfrac{2}{3}\Delta_T^g = 10Dq^g + \tfrac{1}{2}|A_1^E Q_\theta^T| + \tfrac{2}{3}|A_1^T Q_\theta^T| \\
E_3 &= 10Dq^{exc} - \tfrac{1}{2}\Delta_E^{exc} - \tfrac{2}{3}\Delta_T^{exc} = 10Dq^g + |A_{a_{1g}} Q_{a_{1g}}| - \tfrac{1}{2}|A_1^E Q_\theta^E| - \tfrac{2}{3}|A_1^T Q_\theta^E| \\
E_4 &= 10Dq^{exc} - \tfrac{1}{2}\Delta_E^{exc} + \tfrac{1}{3}\Delta_T^{exc} = 10Dq^g + |A_{a_{1g}} Q_{a_{1g}}| - \tfrac{1}{2}|A_1^E Q_\theta^E| + \tfrac{1}{3}|A_1^T Q_\theta^E|
\end{aligned} \tag{2}$$

where

$$A_1^E = \left[\frac{\partial E_{exc}}{\partial Q_{\theta,\varepsilon}}\right]_{O_h} \qquad \text{and} \qquad A_1^T = \left[\frac{\partial E_g}{\partial Q_{\theta,\varepsilon}}\right]_{O_h}$$

are the linear coupling constants for the excited and ground states, respectively. Therefore the JT splittings are

$$\Delta_E^g(R_g) = E_2 - E_1 = |A_1^E Q_\theta^T| \qquad \text{and} \qquad \Delta_T^{exc}(R_{exc}) = E_4 - E_3 = |A_1^T Q_\theta^E|.$$

Taking into account that the equilibrium JT coordinates for $^2T_{2g}$ and ^2E_g are given by $Q_\theta^T = -A_1^T/K_g$ and $Q_\theta^E = -A_1^E/K_{exc}$, respectively, the JT splittings are

$$\Delta_E^g(R_g) = \left|A_1^E Q_\theta^T\right| = \frac{A_1^E A_1^T}{K_g} \qquad \text{and} \qquad \Delta_T^{exc}(R_{exc}) = \left|A_1^T Q_\theta^E\right| = \frac{A_1^T A_1^E}{K_{exc}}. \tag{3}$$

Here, $K_i = \mu\omega_i^2$ is the force constant for the e_g vibration and ω_i is the corresponding angular frequency with $i = g$ and $i = exc$ for the ^2E_g and $^2T_{2g}$ electronic states, respectively. Using vibrational energies for the e_g mode in TiO_6 of $\hbar\omega_T = 239\ cm^{-1}$ (ground state) and $\hbar\omega_E \approx 200\ cm^{-1}$ (excited state) [15], we can explain why the splittings of the excitation and emission bands are similar, although the associated JT distortion for the excited state is higher than for the ground state, $\left|Q_\theta^T\right| < \left|Q_\theta^E\right|$ (figure 3). To account for the difference of $1210\ cm^{-1}$ between the values $\Delta_T^{exc}(R_{exc}) = 1540\ cm^{-1}$ and $\Delta_E^g(R_g) = 2740\ cm^{-1}$, we must consider the variations undergone by the linear coupling parameters, A_1^T and A_1^E, and the vibrational frequencies, ω_T and ω_E, with pressure, as we will see below.

Before doing that, let us analyse the electron–vibrational coupling to the a_{1g} vibration and its influence on the optical spectra. The centroids of the emission and excitation bands are given, respectively, by $E_{excitation} = (E_1 + E_2)/2$ and $E_{emission} = (E_3 + 2E_4)/3$. The difference $E_{SS} = E_{excitation} - E_{emission} = 5430\ cm^{-1}$is directly related to the Stokes shift associated with the totally symmetric a_{1g} distortion (complex volume):

$$E_{SS} = 10Dq^g - 10Dq^{exc} + \tfrac{2}{3}\Delta_T^g + \tfrac{1}{2}\Delta_E^{exc} = \left|A_{a_{1g}} Q_{a_{1g}}\right| + \tfrac{2}{3}|A_1^T Q_\theta^T| - \tfrac{1}{2}\left|A_1^E Q_\theta^E\right|$$
$$\approx \frac{A_{a_{1g}}^2}{K_{a_{1g}}} + 1$$
$$2\frac{A_1^{E^2}}{K-exc} = 2S_{a_{1g}}\hbar\omega_{a_{1g}} + s_{eg}^E\hbar\omega_{exc}. \tag{4}$$

This expression is derived on the assumption that the vibrational frequencies, $\omega_{a_{1g}}$, for the ground and excited states are the same (linear approximation) and $10Dq$ is an order of magnitude higher than the JT splitting whose contribution to E_{SS} is only about 28% ($E_{SS} = 1540\ cm^{-1}$. The parameter $A_{a_{1g}}$ represents the corresponding linear electron–vibrational coupling:

$$A_{a_{1g}} = \left(\frac{\partial 10Dq}{\partial Q_{a_{1g}}}\right)_{Q_{a_{1g}}=0} \tag{5}$$

where $Q_{a_{1g}} = \frac{1}{\sqrt{6}}\sum_{i=1}^{6}\Delta R_i$ is the totally symmetric normal coordinate, and $\Delta R_i = R_i - R_{O_i}$ is the variation of the Ti–O_i distance of the ith oxygen ligand with respect to the ground-state equilibrium geometry, R_{O_i}. $K_{a_{1g}}$ is the force constant, which is related to $\omega_{a_{1g}}$ by $\omega_{a_{1g}}^2 = K_{a_{1g}}/\mu$, where μ is the oxygen mass. The Huang–Rhys parameter is $S_{a_{1g}} = A_{a_{1g}}^2/2\hbar\omega_{a_{1g}}^3\mu$ [27, 29]. This is a good approximation provided that the experimental variation between the ground- and excited-state vibrational energies is $(\omega_{a_{1g}}^{exc} - \omega_{a_{1g}}^g)/\omega_{a_{1g}}^g \leqslant 0.1$ for TM complexes [30].

In conclusion, the total contributions to the Stokes shift, $E_{SS}(a_{1g}) = 2S_{a_{1g}}\hbar\omega_{a_{1g}}$ and $E_{SS}(e_g) \equiv \frac{1}{2}\left[\left|A_1^E Q_\theta^E\right| + \frac{4}{3}\left|A_1^T Q_\theta^T\right|\right] = S_{eg}^E\hbar\omega_{exc} + \frac{4}{3}S_{exc}^T + \frac{4}{3}\hbar\omega_g$, can be measured as a function of the crystal volume by optical spectroscopy under pressure.

Figures 4 and 5 also clearly show that the JT splitting associated with the two electronic states decreases upon application of pressure, while the Stokes shift contribution for the a_{1g} vibration, $E_{SS}(a_{1g})$, increases. This is noteworthy, since no evidence of any increase of the Stokes shift with increasing pressure has been reported so far. In contrast, a decrease of the Stokes shift was observed upon volume reduction in MnF_6^{4-} through the ABF_3:Mn^{2+} perovskite compound series [30, 31], and in $MnCl_6^{4-}$ through the $ABCl_3$:Mn^{2+} series [32, 33], whose chemical pressure effect provides metal–ligand distance variations of 0.27 Å (from $CsCaF_3$ to $KMgF_3$) and 0.33 Å (from $SrCaCl_3$ to $KMgCl_3$) through the series, respectively [31, 33]. A similar behaviour has also been observed in Cr^{3+}-doped chloroelpasolites [34–36]. The opposite (or anomalous) behaviour of the Stokes shift upon increasing pressure observed in Al_2O_3:Ti^{3+}, can be explained on the basis of the configurational diagrams of figure 3(a). If we assume variations of the linear electron–vibration coupling with volume (or R) as

$A_{a_{1g}} = \partial 10Dq/\partial R \propto R^{-(n+1)}$, where $10Dq \propto R^{-n}$ and $\omega \propto R^{-3\gamma}$, then $Q_{a_{1g}} \propto R_g^{-(n+1-6\gamma)}$. Therefore the equilibrium geometry for the excited ^2E_g state as a function of the Ti–O distance R_g is given by $R_{exc} = R_g + \Delta R$, with $\Delta R = \frac{1}{\sqrt{6}} Q_{a_{1g}} \propto R_g^{-(n+1-6\gamma)} = R_g^{-6(1-\gamma)}$ for $n = 5$ [22]. This estimate implies a reduction of ΔR upon increasing the pressure provided that $\gamma > 1$, as is usually found for the totally symmetric mode in TM complexes [19, 37]. The contribution of this mode to the Stokes shift is then

$$E_{SS}(a_{1g}) = |A_{a_{1g}} Q_{a_{1g}}| \propto R_g^{-2(n+1-3\gamma)} = R_g^{-6(2-\gamma)}.$$

Taking $\gamma \approx 1.31$, we can explain why $E_{SS}(a_{1g})$ increases with increasing pressure (reduction of R_g), as observed in figure 5.

Analogously, the variation of the JT splitting for the ^2E_g and $^2T_{2g}$ states with R_g can be deduced on the assumption that the linear electron–e_g vibration coupling parameters show the proportionalities $A_1^T \propto R_g^{-(n_T+1)}$, $A_1^E \propto R_{exc}^{-(n_E+1)}$ with $n_E < n_T$ [38]. Theoretical calculations on the variation of A_1^E with the metal–ligand distances carried out on different JT complexes result in values of $n_E \approx 4$. This coincides with the point-charge crystal-field model value [39]. Then the JT splittings as functions of the ground- and the excited-state equilibrium geometries, R_g and R_{exc}, are given by

$$\begin{aligned} \Delta_E^g(R_g) &= \frac{A_1^E A_1^T}{K_g} \propto \frac{R_g^{-(n_E+1)} R_g^{-(n_T+1)}}{\omega_g^2} \\ \Delta_T^{exc}(R_{exc}) &= \frac{A_1^T A_1^E}{K_{exc}} \propto \frac{R_{exc}^{-(n_T+1)} R_{exc}^{-(n_E+1)}}{\omega_{exc}^2}. \end{aligned} \tag{6}$$

Provided that $R_{exc} = R_g + \Delta R$ with $\Delta R = \frac{1}{\sqrt{6}} Q_{a_{1g}}$ and $Q_{a_{1g}} = -A_{a_{1g}}/K_{a_{1g}} = -A_{a_{1g}}/\mu\omega_{a_{1g}}^2$, we then obtain

$$\begin{aligned} A_{a_{1g}} = \left(\frac{\partial 10Dq}{\partial R}\right)_{R_g} &= -5\frac{10Dq}{R_g} = -5 \times \frac{19\,130}{1.9} = -50\,340 \text{ cm}^{-1} \text{ Å}^{-1} \\ &= -9.98 \times 10^{-9} \text{ J m}^{-1}. \end{aligned}$$

By use of $10Dq \propto R_g^{-5}$, $\mu = 2.66 \times 10^{-26}$ kg and taking $\omega_{a_{1g}} = 9.7 \times 10^{13}$ s^{-1} ($\hbar\omega_{a_{1g}} = 515.3$ cm^{-1}) [40], we obtain

$$\Delta R = \frac{1}{\sqrt{6}} \frac{9.98 \times 10^{-9}}{2.66 \times 10^{-26}(9.7 \times 10^{13})^2} = 0.16 \text{ Å} \qquad R_{exc} = 1.9 + \Delta R = 2.06 \text{ Å}.$$

At ambient pressure, we use vibrational frequencies for the e_g mode of 239 and 200 cm^{-1} for the ground and excited state, respectively. For the sake of simplicity, we use $n_T = n_E = 4$, and we find a relationship between their corresponding JT splittings from equation (6):

$$\frac{\Delta_E^g(R_g)}{\Delta_T^{exc}(R_{exc})} \equiv \left(\frac{\omega_{exc}}{\omega_g}\right)^2 \left(\frac{R_g}{R_{exc}}\right)^{-(n_E+n_T+2)} = \left(\frac{200}{239}\right)^2 \left(\frac{1.9}{2.06}\right)^{-10} = 1.57.$$

This value is in good agreement with the experimental ratio $\Delta_E^g(R_g)/\Delta_T^{exc}(R_{exc}) \approx 1.8$ at ambient pressure. This ratio equals 1.8 if we assume an empirical exponent $n_T = n_E = 4.8$. Therefore the smaller JT splitting observed in emission can be reasonably accounted for by the present model.

However, the situation is rather different for the pressure dependencies of $\Delta_E^g(P)$ and $\Delta_T^{exc}(P)$ shown in figure 5. The pressure variation of the former parameter is given by $\Delta_E^g(R_g) \propto A_1^E A_1^T \omega_g^{-2} \propto R_g^{-(n_E+n_T+2-6\gamma')}$ where γ' is the Grüneisen parameter associated with the local e_g vibration.

Using the same values of $n_T = n_E = 4$, we conclude that a reduction of $\Delta_E^g(R_g)$ with pressure is possible provided that $\gamma' > (n_E + n_T + 2)/6 = 1.7$. Since we observe a decrease of Δ_E^g and Δ_T^{exc} with P, it seems likely that we can assume γ'-values slightly higher than the critical value $\gamma' = 1.7$. The relative variation of $\Delta_E^g(R_g)$ is then

$$\frac{\delta\Delta_E^g(R_g)}{\Delta_E^g(R_g)} = -(n_E + n_T + 2 - 6\gamma')\frac{\partial R}{\partial P}\frac{\delta P}{R} = (n_E + n_T + 2 - 6\gamma')\frac{\delta P}{3B_0}. \quad (7)$$

It follows that

$$\frac{\partial\Delta_E^g(R_g)}{\partial P} = (n_E + n_T + 2 - 6\gamma')\frac{\Delta_E^g(R_g)}{3B_0}. \quad (8)$$

Here, we used the crystal bulk modulus instead of the local one, with the aim of scaling dependences of the JT coupling constants and the Grüneisen parameters to variations of the crystal volume, and not to local changes.

Using experimental values of $\partial\Delta_E^g(R_g)/\delta P = -1.66\ \mathrm{cm}^{-1}\ \mathrm{kbar}^{-1}$ and $B_0 = 2510$ kbar, we obtain

$$\gamma' = \frac{1}{6}\left(n_E + n_T + 2 - \frac{3 \times 2510 \times (-1.66)}{2740}\right) = 2.43.$$

The present model is also able to explain the smaller pressure shift of $\Delta_T^{exc}(R_{exc})$ in comparison to the pressure shift of $\Delta_E^g(R_g)$. According to equation (7), the partial derivatives $\partial\Delta_E^g(R_g)/\delta P$ and $\partial\Delta_T^{exc}(R_{exc})/\delta P$ are proportional to the JT splittings $\Delta_E^g(R_g)$ and $\Delta_T^{exc}(R_{exc})$, respectively. The corresponding shift rates are expected to exhibit proportional ratios if we assume that the bulk modulus is the same for the ground as for the excited state. The experimental pressure shift rates of 1.66 and 0.53 $\mathrm{cm}^{-1}\ \mathrm{kbar}^{-1}$ approach the experimental $\Delta_E^g(R_g)$ and $\Delta_T^{exc}(R_{exc})$ splitting ratios at ambient pressure.

We interpret the pressure-induced enhancement of the lifetime as being related not to a modification of the Al^{3+} host symmetry, but to a decrease of the transition oscillator strength owing to a blue-shift experienced by the intensity-enabling $O^{2-} \rightarrow Ti^{3+}$ charge-transfer (CT) states. In fact, it is well known that the CT energy in O_h complexes should increase upon increasing the pressure, as a consequence of the destabilization of the 3d levels due to a reduction of R_g (the Ti–O distance) [28, 41]. A similar situation has recently been found in Mn^{2+}-doped fluorites [42]. The parity-forbidden electric dipole transitions in TM complexes are released through coupling to odd-parity vibrations. Odd vibrations break down the centre of inversion, thus allowing coupling to CT states of odd parity. The oscillator strength enhancement by this mechanism is thermally activated. Within a perturbation scheme, the oscillator strength is proportional to $|\langle\Gamma_u^{CT}|H_{odd-vib}|E_g\rangle|^2/(E_{CT} - E_0)^2$, where Γ_u^{CT} represents the odd-symmetry-coupled CT state and $H_{odd-vib} = \partial V_{CT}/\partial Q_{odd}$ is the corresponding linear electron–vibration coupling. Therefore, we are able to explain the pressure enhancement of the lifetime in terms of an increase of $(E_{CT} - E_0)^2$. The rise of the CT energy with pressure is due to an increase of the repulsion interaction of the ligand electrons induced by a reduction of the O^{-2}–Ti^{3+} distance.

5. Concluding remarks

The present results confirm that the excitation and emission of Al_2O_3:Ti^{3+} under pressure can be explained in terms of a simple model based on electron–vibration couplings to vibrations of a_{1g} and e_g symmetries. The Stokes shift related to the a_{1g} mode, the JT splitting, and their variations with pressure are well described by this model, if pressure dependencies of the

electron–vibration couplings $A \propto R^{-(n+1)}$ with $n \approx 4$–5 are assumed. The increase of the a_{1g} Stokes shift under pressure and the opposite dependence of the JT splitting on pressure are justified by assuming Grüneisen parameters $\gamma < 2$ for the a_{1g} vibration and $\gamma' > 1.7$ for the JT e_g vibration.

The application of pressure to Al_2O_3:Ti^{3+} provides an increase of the Stokes shift and the lifetime, thus *potentially* improving the laser capability of this material.

Acknowledgments

We are indebted to the Vicerrectorado de Investigación of the University of Cantabria and the CICYT (Project No PB98-0190) for financial support. We thank the Institute for Single Crystals, Kharkov, Ukraine, for providing the Al_2O_3:Ti^{3+} sample.

References

[1] Moulton P F 1982 *Opt. News* **8** 9
[2] Bantien F, Albers P and Huber G 1987 *J. Lumin.* **36** 363
[3] Wegner T and Petermann K 1989 *Appl. Phys.* B **49** 275
[4] Rodríguez F, Riesen H and Güdel H U 1991 *J. Lumin.* **50** 101
[5] Moulton P F 1985 *Laser Handbook* (Amsterdam: Elsevier)
[6] Okhrimchuk A G and Shestakov A V 1994 *Opt. Mater.* **3** 1
[7] Merkle L D, Pinto A, Verdum H R and McIntosh B 1992 *Appl. Phys. Lett.* **61** 2387
[8] Weakliem H A and McClure D S 1962 *J. Appl. Phys.* **33** 347
[9] McClure D S 1962 *J. Chem. Phys.* **36** 2757
McClure D S 1962 *J. Chem. Phys.* **37** 1571 (erratum)
[10] Sturge M D 1967 *Solid State Physics* vol 20 (New York: Academic) p 91
[11] Englman R 1972 *The Jahn–Teller Effect in Molecules and Crystals* (New York: Wiley-Interscience)
[12] Powell R C, Venikouas G E, Xi L, Tyminski J K and Kokta M R 1986 *J. Chem. Phys.* **84** 662
[13] Henderson B and Imbusch G K 1989 *Optical Spectroscopy of Inorganic Solids* (Oxford: Clarendon)
[14] Albers P, Stark E and Huber G 1986 *J. Opt. Soc. Am.* B **3** 134
[15] Grinberg M, Mandelis A, Fjeldsted K and Othonos A 1993 *Phys. Rev.* B **48** 5922
[16] Grinberg M, Mandelis A and Fjeldsted K 1993 *Phys. Rev.* B **48** 5935
[17] Minomura S and Drickamer H G 1961 *J. Chem. Phys.* **35** 903
[18] Jia W, Liu H, Lim K and Yen W M 1989 *J. Lumin.* **43** 323
[19] Ferraro J R 1984 *Vibrational Spectroscopy at High External Pressures: the Diamond Anvil Cell* (Orlando, FL: Academic)
[20] Wenger O S and Güdel H U 2001 *J. Chem. Phys.* **114** 5832
[21] Wenger O S, Valiente R and Güdel H U 2001 *J. Chem. Phys.* **115** 3819
[22] Drickamer H G and Frank C W 1973 *Electronic Transitions and the High Pressure Chemistry and Physics of Solids* (London: Chapman and Hall)
[23] Watson G H Jr, Daniels W B and Wang C S 1981 *J. Appl. Phys.* **52** 956
[24] Duclos S J, Vohra Y K and Ruoff A L 1990 *Phys. Rev.* B **41** 5372
[25] Zheng W 1996 *Phys. Status Solidi* b **196** 297
[26] Zheng W 1995 *J. Phys.: Condens. Matter* **7** 8351
[27] Rodríguez F, Nuñez P and Marco de Lucas M C 1994 *J. Solid State Chem.* **110** 370
[28] Valiente R and Rodríguez F 1999 *Phys. Rev.* B **60** 9423
[29] Fowler W B 1968 *Physics of Color Centers* (New York: Academic) p 72
[30] Marco de Lucas M C, Rodríguez F and Moreno M 1995 *J. Phys.: Condens. Matter* **7** 7535
[31] Marco de Lucas M C, Rodríguez F and Moreno M 1994 *Phys. Rev.* B **50** 2760
[32] Marco de Lucas M C, Rodríguez F, Güdel H U and Furer N 1994 *J. Lumin.* **60+61** 581
[33] Marco de Lucas M C, Rodríguez F, Prieto C, Verdaguer M and Güdel H U 1995 *J. Phys. Chem. Solids* **56** 995
[34] Dolan J F, Rinzler A G, Kappers L A and Bartram R H 1992 *J. Phys. Chem. Solids* **53** 905
[35] Rinzler A G, Dolan J F, Kappers L A, Hamilton D S and Bartram R H 1993 *J. Phys. Chem. Solids* **54** 89
[36] Woods A M, Sinkowits R S, Charpie J C, Huang W L, Bartram R H and Rossi A R 1993 *J. Phys. Chem. Solids* **54** 543

[37] Holzapfel W B and Isaacs N S 1997 *High-Pressure Techniques in Chemistry and Physics. A Practical Approach* (New York: Oxford University Press)
[38] Aguado F, Rodríguez F and Núñez P 2002 *Proc. EHPRG'39* at press
[39] Barriuso M T, Aramburu J A and Moreno M 1996 *Phys. Status Solidi* b **196** 193
[40] Sekiya T, Ohta S, Kamei S, Hanakawa M and Kurita S 2001 *J. Phys. Chem. Solids* **62** 717
[41] Moreno M, Barriuso M T and Aramburu J A 1992 *Appl. Magn. Reson.* **3** 283
[42] Rodríguez F, Hernández I, Gutiérrez R E, García-Revilla S, Moreno M and Alcalá R 2002 *Proc. EHPRG'39* at press